High electrical conductivity and π-π stacking interface design for tunable electromagnetic wave absorption composite foams

Wen-Hong Jiang,[a] Bo Jiang*[a], Jian Yang[a], Ming Qiang Wang[a,b], Ying Li[a]

a MIIT Key Laboratory of Critical Materials Technology for New Energy Conversion

and Storage, School of Chemistry and Chemical Engineering, Harbin Institute of

Technology, China. E-mail: jiangbo5981@hit.edu.cn (B. Jiang).

b Jiangsu Province Key Laboratory of Fine Petrochemical Engineering,Changzhou

University, Changzhou 213164, China

Experimental Section

Preparation of Fe$_3$O$_4$-NH$_2$

Fe$_3$O$_4$ (4 g，20 mmol), APTES (8 mL, 40 mmol) was dissolved in deionized (DI) water (140 mL) and ethanol (60 mL) and stirred at 40°C for 2 h. Fe$_3$O$_4$-NH$_2$ was collected by magnet and dried at 60 °C.

Preparation of CNT- Fe$_3$O$_4$

CNTs (200 mg) were put into 50 mL solution (35 mL deionized water and 15 mL ethanol) and ultrasonicated for 30 min. Fe$_3$O$_4$-NH$_2$ (1.0 g) was added into the CNTs suspension and vigorously stirring for 2 h at 70°C, the CNT- Fe$_3$O$_4$ has been preparate.

Preparation of RT prepolymer

The RT prepolymer was prepared with resorcinol (R) (1.10 g, 10 mmol) and terephthalaldehyde (T) (1.34 g, 10 mmol) and stirred in ethylene glycol (EG) (1 mL) and acetic acid (HAc) (1 mL) at 120°C for 2 h. The resulting prepolymer was continuously cured at 150°C for 2 h and at 180°C for 2h.

The conductivity tests

The DC electrical conductivity of composites with size of 15 × 5 × 5 mm was calculated according to the following formula: σ= L/RS[1-5]. (where R is the electrical resistance, L is the length, and S is the area of the sample). R was measured using a digital multimeter. A minimum of five measurements were obtained for an average value.

The preparation of the EMA test sample

An Agilent E5071C vector network analyzer (Agilent, USA) was applied to determine the relative permeability and permittivity in the frequency range of 2-18 GHz for the calculation of reflection loss. The obtained composites were processed into a ring with an outer diameter of 7 mm, an inner diameter of 3 mm, and a thickness of 3.5 mm for microwave measurement.

S1. SEM image of the RTFs

Fig. S1 shows the photographic image of the RTFs which was synthesized with salt template. The SEM image demonstrate the size of pore was the size of salt. The nanomaterials of CNT-Fe_3O_4/PPD were adhesive on the resin surface, which can be observed in the high magnification image. The rough surface in the figure was a combination of nanomaterials and resin, smooth place was fracture surface of pure resin, which can clearly observe the pore structure of CNT-Fe_3O_4/PPD/RT. The high magnification image of rough surface can observe composite structure of CNT-Fe_3O_4 and resin. Linear structure was CNT-Fe_3O_4, the pore diameter of composites was the salt grain diameter which was distributed from 168 to 389 μm.
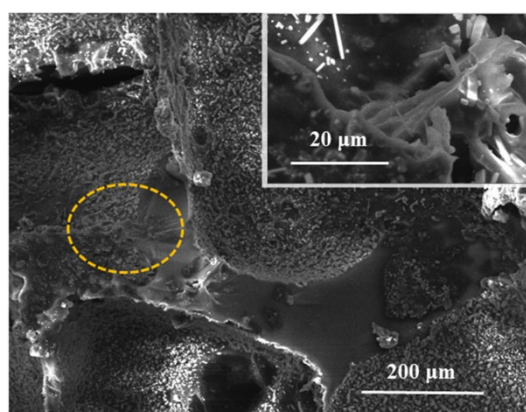
**Fig. S1.** SEM image of the RTFs.

S2. XPS curves of CNT-Fe_3O_4/PPD

The peaks at 55.3 eV, 711.3 eV and 724.3 eV were corresponded to the representative of Fe_{3P}, $Fe_{2P3/2}$ and $Fe_{2P1/2}$ as shown in Fig. S2. From these evidences above, it demonstrates CNT-Fe_3O_4/PPD were successfully fabricated.
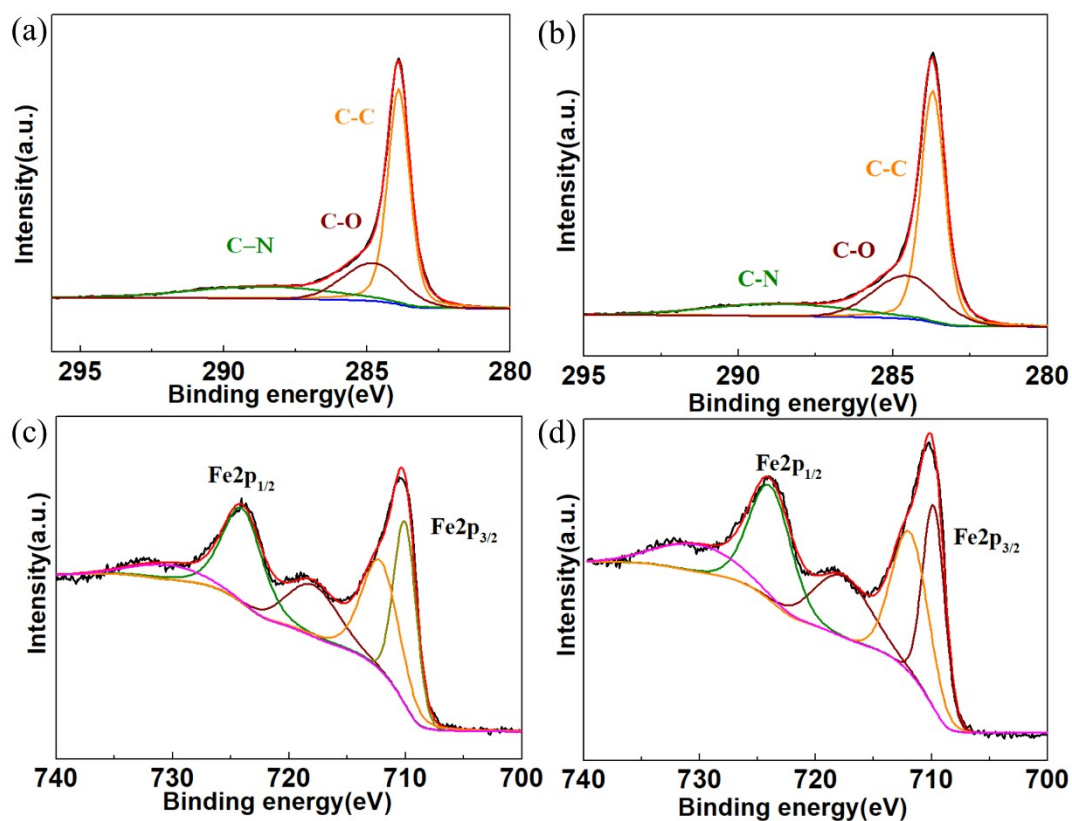
Fig. S2. XPS spectra of CNT- Fe_3O_4/PDA (a, c) and CNT- Fe_3O_4/PPD (b, d).
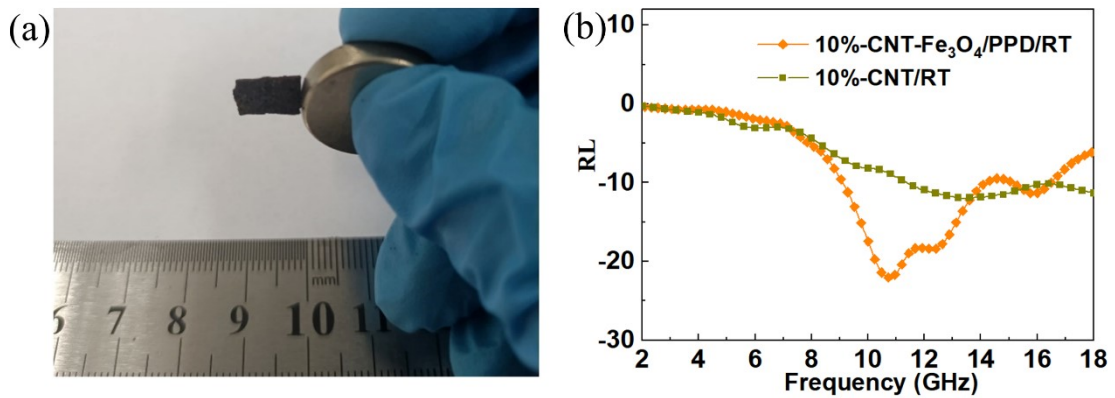
S3. FT-IR spectra of CNT-Fe_3O_4/PPD/RT and CNT-Fe_3O_4/RT.

The characteristic peaks of the RT resin are still reserved in composites. Interestingly, the peak of the C = O vibration in CNT-Fe_3O_4/RT composites moved to a lower position (804 – 834 cm^{-1}) than CNT-Fe_3O_4/ PPD/RT. The change of C = O peak implies the variation of the electronic conjugation in the composites, which is essential to the intermolecular π-π interaction and hence boosts the delocalization of the electrons[6]. It reveals the π-π stacking interactions between RT and CNT-Fe_3O_4/PPD.
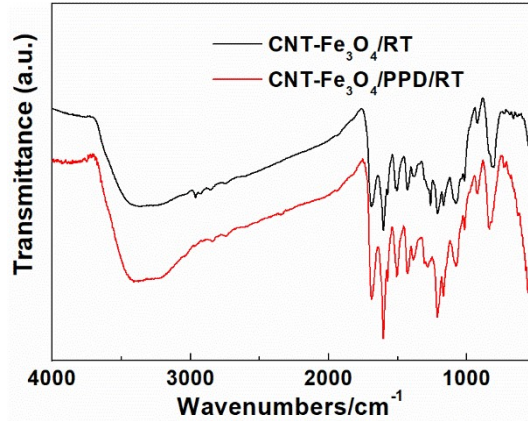
Fig. S3. FT-IR spectra of CNT-Fe$_3$O$_4$/PPD/RT and CNT-Fe$_3$O$_4$/ RT.

## S4. EMA of CNT-Fe$_3$O$_4$/PPD/RT and CNT/RT.

In Fig. S4(a), The composites can be adsorbed on the magnet, which proving the existence of ferric oxide. The electromagnetic spectrum of the reflection of CNT/RT was tested in Fig. S4(b). For the composites of CNT/RT, the minimum RL coefficient was -12.02 dB. The lower minimum RL coefficient of CNT-Fe$_3$O$_4$/PPD/RT was attribute to the Fe$_3$O$_4$ nanoparticle absorption can attenuate the skin effect of conductive materials. Meanwhile, heterogeneous interfaces of CNT-Fe$_3$O$_4$/PPD were beneficial to the EMA.

Fig. S4. (a)The image of the CNT-Fe$_3$O$_4$/PPD/RT. (b) Frequency dependence of microwave reflection loss for CNT-Fe$_3$O$_4$/PPD/RT and CNT/RT.

## S5. impedance matching characteristic of CNT-Fe$_3$O$_4$/PPD/RT

Fig. S5 depicts the Z versus frequency curves. when Z is close to 1 implies an excellent impedance matching characteristic, which indicates that the incident EM wave can effectively penetrate into absorption composites. Obviously, the Z (Z = $|Z_{in}/Z_0|$) values stay away from 1.0 for composites with CNT-Fe$_3$O$_4$/PPD/RT, for RTFs, impedance matching and attenuation losses gradually deteriorate with increasing nanomaterial additions. The main reason for this phenomenon is that the increased electrical conductivity of composites result in increased reflection of incident electromagnetic waves.
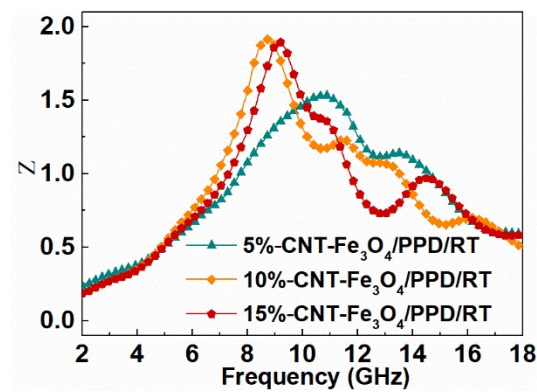
Fig. S5. Frequency-dependent Z of CNT-Fe$_3$O$_4$/PPD/RT

S6. Frequency-dependent RL curves of CNT-Fe$_3$O$_4$/PPD/RT in different thick

The minimum reflection loss (RL) and the wide effective absorption bandwidth changed with the increase of the thickness of foams. The foams showed a wide effective absorption bandwidth at 9.68−18 GHz and reached the minimum RL value of −33 dB at 14.24 GHz with a thickness of 3.5 mm. RTFs shows two peaks, wide effective absorption bandwidths at 9.12-10.88 and 12.88-14.88 GHz, and reached the minimum RL values of −16 dB at 10.16 GHz and −17 dB at 14 GHz with a thickness of 4.5 mm.
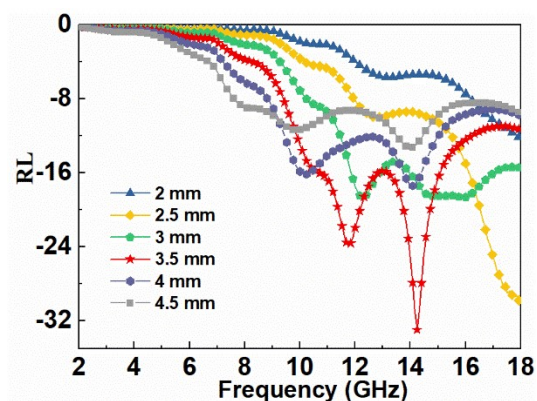
Fig. S6. Frequency-dependent RL of CNT-Fe$_3$O$_4$/PPD/RT.

S7. TG curve of RTFs.

Fig. S7 shows the TG plot for pristine RTF-CNT-10, RTF-5, RTF-10 and RTF-15 in nitrogen atmosphere. In the first step, up to a temperature of 100 °C, the weight loss can be attributed to the evaporation of the water. The second step from 150 to 600 °C can be attributed to the degradation of RT. Finally, at temperatures above 800°C may be explained by degradation of the thermal oxidation of the remaining disordered carbon and the elimination of oxcygen element of Fe$_3$O$_4$ attached to the CNT walls. On the contrary, the plot for RTFs shows a sharp degradation at about 800 °C, which can be attributed to the degrdation of the grafted Fe$_3$O$_4$ on CNT. This also demonstrates the susscessful grafting of Fe$_3$O$_4$ on to CNTs.
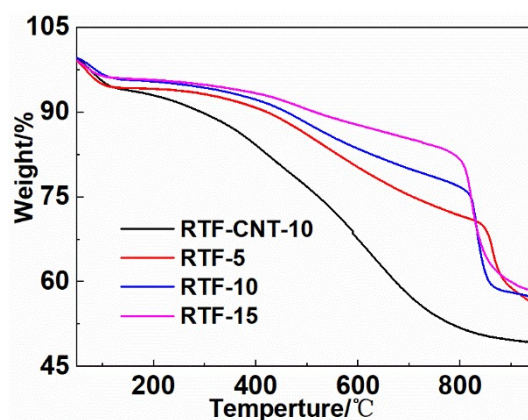
Fig. S7. TG curves of the RTFs.

1. L.M. Zhang, Y. He, S. Cheng, H. Sheng, K. Dai, W.J. Zheng, M.X. Wang, Z.S. Chen, Y.M. Chen, Z. Suo, Small 2019, 15, e1804651.

2. L. Liang, P. Xu, Y. Wang, Y. Shang, J. Ma, F. Su, Y. Feng, C. He, Y. Wang, C. Liu, Chem. Eng. J. 2020, 395.

3. M. Zhou, J. Wang, Y. Zhao, G. Wang, W. Gu, G. Ji, Carbon 2021, 183, 515.

4. J. Zheng, X. Wei, Y. Li, W. Dong, X. Li, S. E, Z. Wu, J. Wen, Nano Energy 2021, 89.

5. Y.-S. Jun, B.G. Hyun, M. Hamidinejad, S. Habibpour, A. Yu, C.B. Park, Compos. Part B 2021, 223.

6. R. Tang, D. Gong, Y. Deng, S. Xiong, J. Deng, L. Li, Z. Zhou, J. Zheng, L. Su, L. Yang, Chem. Eng. J. 2022, 427.